



Investigation of light effects on $Fe/(111)$ n-type $Si_{0.65}Ge_{0.35}$ using current-voltage and impedance spectroscopy

Abdelkader Teffahi^{a,*}, Djillali Hamri^b, Asma Djeghlouf^c, Abdelkader Mostefa^b, Mahmoud Arbid^a, Souleyman Benkraouda^a, Abdelmadjid Mesli^d

^a Applied Science Laboratory, National Higher School of Advanced Technologies, Algiers, Algeria

^b Industrial Engineering and Sustainable Development Laboratory GIDD, Department of Electrical Engineering and Automation, Relizane University, Relizane, Algeria

^c Department of Electronics, Faculty of Technology, Hassiba Benbouali University of Chlef, Chlef, Algeria

^d Institut Matériaux Micro électronique Nanosciences de Provence, UMR6242CNRS, Université Aix-Marseille, Av. Normandie-Niemen, 13397, Marseille, Cedex20, France

ARTICLE INFO

Keywords:

$Fe/Si_{1-x}Ge_x$
Schottky
diode
Impedance spectroscopy
Light effect
Surface states density
Conductivity (σ_{ac})

ABSTRACT

Light induced effects at the interface of $Fe/n-Si_{0.65}Ge_{0.35}$ (MS) Schottky barrier diodes are study by reverse and forward bias current-voltage ($I-V$) and impedance spectroscopy measurements at room temperature and for 50–1000 kHz frequency range. Ideality factor (n), series resistance and shunt resistance (R_s , R_{sh}), barrier height shows that Poole-Frenkel-type current is the most important portion of dark reverse current and Schottky-type current under illumination. surface states density (N_{SS}) was strongly light dependent. Real and imaginary portions of complex impedance (Z' , Z''), complex electric modulus (M' , M'') and conductivity (σ_{ac}) were also found to depend on light intensity and frequency. Z'' and M'' behaviors with light and frequency reveal relaxation processes taking place at metal- $Si_{1-x}Ge_x$ junction. Arrhenius law of extracted relaxation time led to the calculation of activation energy. The behaviors of the $\ln(\sigma_{ac})$ vs $1/P$ plots confirmed the presence of two distinct conduction mechanisms corresponding to low and high illumination intensities.

1. Introduction

Schottky contact Diodes (SBDs) are the simplest electronic devices made of metal-semiconductor (MS) [1,2]. The interface plays a major role in their performance, reliability, and stability [1,3,4]. Proper MS contact is crucial to ensure efficient use of these devices [5]. For more than two decades, $Si_{1-x}Ge_x$ has attracted intense scientific interest due to its potential applications in optoelectronics and high-speed electronic devices, as well as its compatibility with current silicon technology [6, 7]. Varying the concentration of germanium (Ge) allows controlling its band gap, which enables the fabrication of many devices such as heterojunction bipolar transistors (HBTs), infrared detectors, and modulation-doped field-effect transistors (MODFETs) [3–5,8]. In order to grasp high-performance Schottky devices, it is necessary to have a thorough understanding of electronics.

A precise understanding of electrical characteristics and conduction mechanisms is essential to understand high-performance Schottky devices. This refers to the flow of electrons over the barrier between the metal and the semiconductor when a voltage is applied. Therefore, the

production of high-performance semiconductors using $Si_{1-x}Ge_x$ mainly rely on the quality of the contact between the metal and $Si_{1-x}Ge_x$. It is beneficial to study the characteristics of this contact for different metals and under different conditions in order to gain a better understanding and more effective control of the electrical characteristics.

Impedance spectrometry (IS) is an electrical method used to monitor the electrical response when an electric current is applied as a function of frequency. It is a powerful electrical measurement technique used in many fields, such as materials science, electrochemistry, semiconductor industry, sensors, biology, and medicine. Various electrical parameters can be obtained by measuring the complex impedance at different frequencies. It allows to distinguish various effects that contribute to a measurement and, by using advanced mathematical methods, it is possible to calculate inaccessible quantities. With the IS method, it is possible to observe the electrical characteristics of the bulk and the interface, which cannot be observed with direct current (dc) methods because the electric response for each component differs on a microscopic time scale.

Modulus spectroscopy is known to be a good dielectric technique to

* Corresponding author.

E-mail address: abdelkader.teffahi@ensta.edu.dz (A. Teffahi).

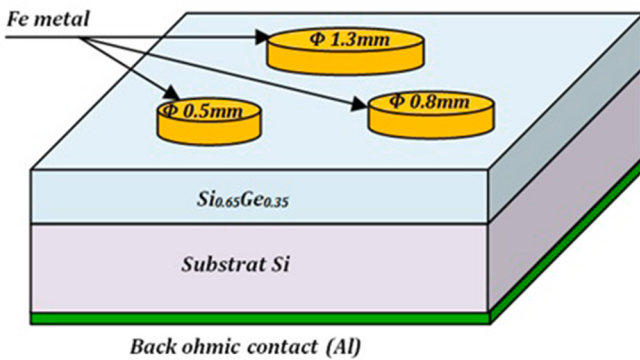


Fig. 1. Schematic diagram of Fe/n-Si_{0.65}Ge_{0.35} Schottky barrier diodes.

extract hidden relaxation processes [9]. This method has been widely employed to study the electrical characteristics of MIS and MS contacts [10,11], and it offers diagnostic suggestions for device improvement. Nowadays, illumination intensity has been one of the most common processes to modify morphological, electronic, optoelectronic, and dielectric structures [12–15]. The illumination intensity technology has technological significance for many applications in semiconductor electronic devices. According to our best knowledge, there is no research on the electrical characteristics related to illumination of iron on n-type Si_{1-x}Ge_x. In this paper, electrical and interface properties of Fe/Si_{0.65}Ge_{0.35} Schottky contacts are studied using *I-V* characteristics, impedance and modulus spectroscopy for illumination intensities in the range 50–400 mW/cm² and 50–1000 kHz frequency range. Obtained results show the strong effect of illumination intensity and frequency on the complex impedance (Z' , Z''), electric modulus (M'') and ac electrical conductivity (σ_{ac}) of such Schottky contacts.

2. Experimental details

Using molecular beam epitaxy (MBE) a layer of *n*-Si_{1-x}Ge_x (x = 35 %) was grown with Antimony ($N_D = 3\text{--}4 \times 10^{15} \text{ cm}^{-3}$) doping on Silicon (Si)

at a temperature of 550 °C. Film thickness was 2 μm on 350 μm thick (111) crystal orientated Si substrate of $\leq 0.7 \Omega \text{ cm}$ resistivity. Just after cleaning the surface, high purity (99.999 %) circular Iron (Fe) contacts, 0.5–1.3 mm in diameter and ~0.2 μm thick were thermally evaporated onto the Si_{1-x}Ge_x wafer. This high vacuum metal evaporation took place at a pressure of about 10⁻⁶ Torr. Low resistance ohmic back metal contact was obtained with aluminum metallization of substrate back-side. For more experimental details see Ref. [16]. Fig. 1 illustrates the structure of the device used in this study.

Light intensities in the range 100–400 mW/cm² were obtained using a xenon lamp (24V, 100W) and measured using a light meter. *I-V* characteristics were obtained with an Agilent precision semiconductor parameters analyzer (4156C). Complex impedance real and imaginary parts (R - X) were measured using a Wayne Kerr 6500B precision impedance analyzer. Charge concentration of epitaxial layer, $3 \times 10^{15} \text{ cm}^{-3}$, was checked using capacitance-voltage plots at reverse-bias and 1 MHz frequency using an Agilent LCR meter (4980A).

3. Results and discussion

3.1. Current-voltage (*I-V*) characteristics

Fe/n-Si_{0.35}Ge_{0.65} Schottky diode (*I-V*) plots under various illumination intensities (100–400 mW/cm²) as well as in dark are given in Fig. 2. In dark condition, the Schottky contact has a rectifying ratio (RR) above 10³. Under illumination, such rectifying ratio at (± 0.35 V) drops to 79,

Table 1
Electrical parameters extracted from I-V plot.

Power (mW/cm ²)	Saturation Current (A)	Ideality factor (n)	Barrier height ϕ_{B0} (eV)
Dark	1.14×10^{-9}	1.634	0.842
100	2.21×10^{-7}	1.729	0.705
200	5.27×10^{-7}	1.866	0.682
300	8.78×10^{-7}	1.909	0.669
400	1.05×10^{-6}	1.934	0.664

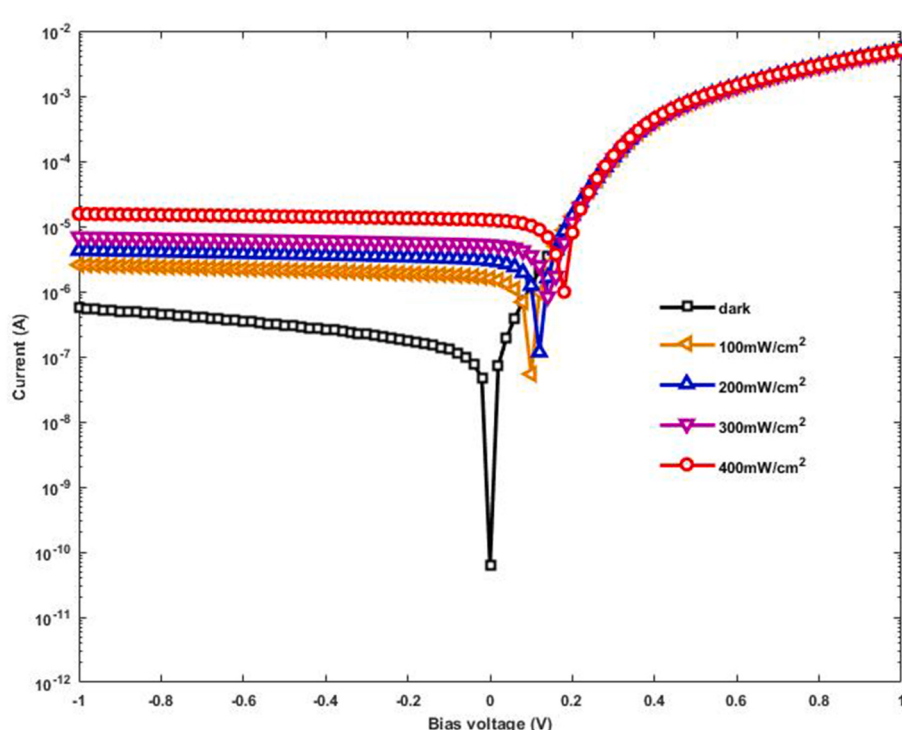


Fig. 2. Forward and reverse bias Fe/n-Si_{0.65}Ge_{0.35} ln(*I*)-V characteristics under various illuminations levels.

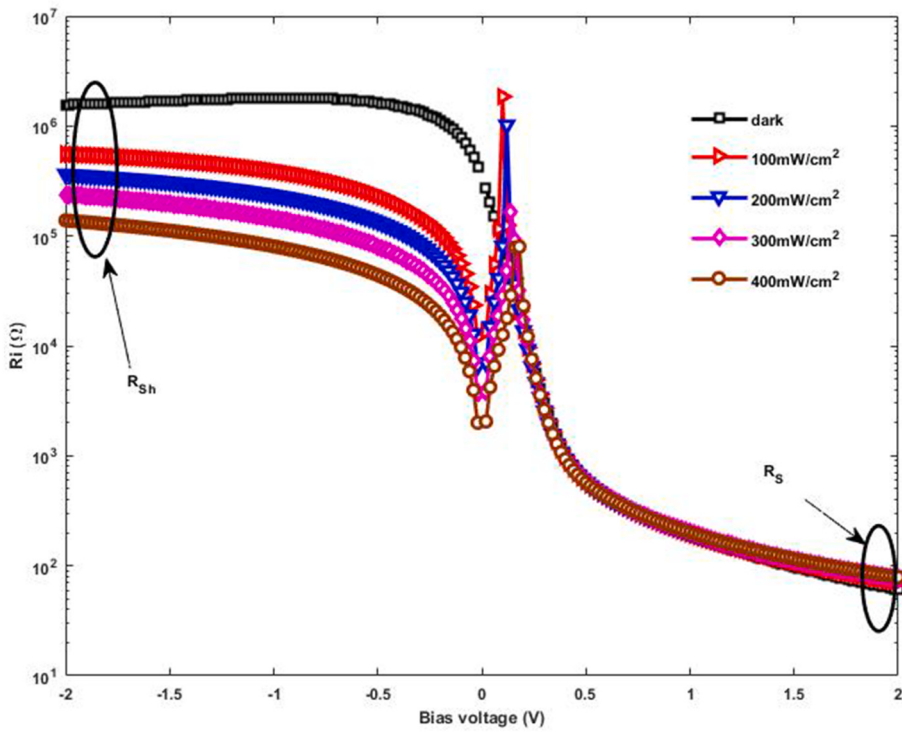


Fig. 3. R_i vs. V plots used to evaluate R_s and R_{sh} in Fe/n-Si_{0.65}Ge_{0.35} SBD.

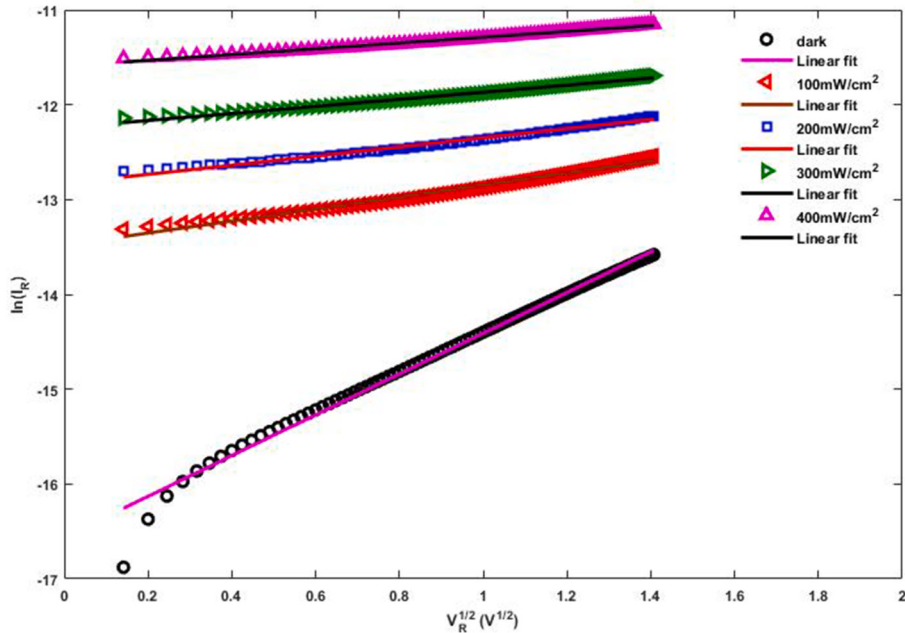


Fig. 4. $\ln(I_R)$ vs $V_R^{1/2}$ plots of Fe/n-Si_{0.65}Ge_{0.35} to find conduction mechanisms.

45, 30 and 25 for 100, 200, 300 and 400 mW/cm², respectively. Such RR decrease with increasing light intensity indicates the strong effect of light intensity on reverse bias. Voltage-current dependence, for the well-known thermionic emission theory, is given as [17,18]:

$$I = I_S [\exp(qV / nkT) - 1] \quad (1)$$

$$\text{With } I_S = AA^* T^2 \exp(-q\phi_{B0} / kT) \quad (2)$$

Where I_S , n , q , T and k are saturation current, ideality factor, charge

electric, temperature in Kelvin and Boltzmann constant, respectively. A , A^* , and ϕ_{B0} are Schottky section, effective Richardson constant, and zero-bias barrier height, respectively. I_S is extracted from the intercept of linear part of $\ln(I)-V$ plot on the y -axis. Barrier height ϕ_{B0} can be expressed as [17]:

Under illumination, the photons with energy higher than that of the semiconductor bandgap can generate electron-hole pairs in depletion region. They would be separated by the strong local internal electric field of the depletion region [19]. The main electrical parameters of the diode in the dark and under different illumination intensities can be

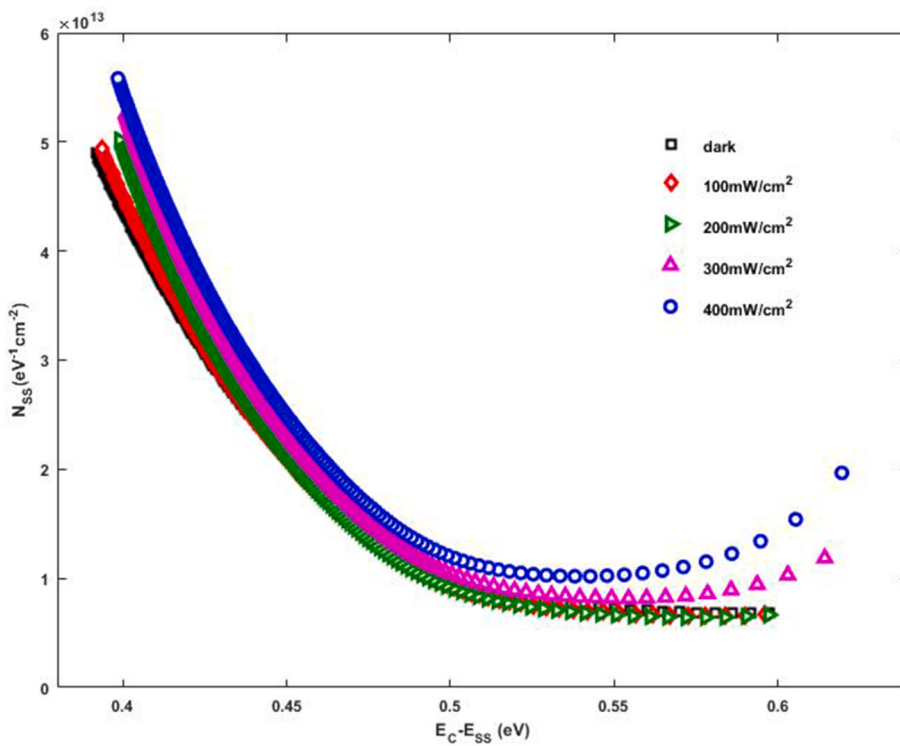


Fig. 5. N_{SS} vs $(E_C - E_{SS})$ plots of Fe/n-Si_{0.65}Ge_{0.35} in dark and under four illumination levels.

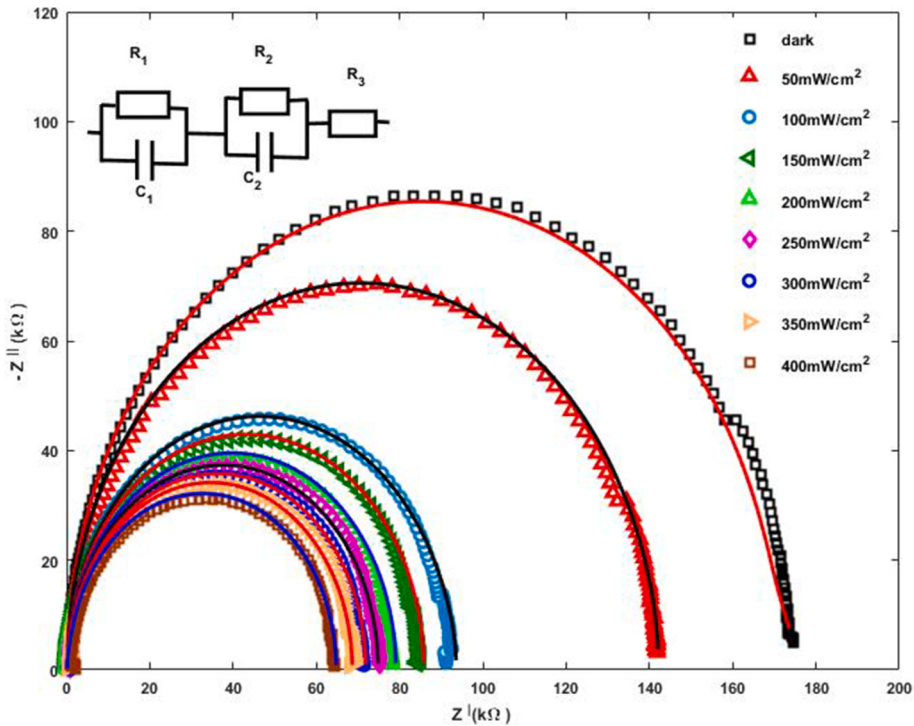


Fig. 6. Cole-Cole plots of Fe/n-Si_{0.65}Ge_{0.35} for various light levels.

obtained from equation (1). The values obtained according to the thermal emission theory are presented in Table 1. It is important to emphasize that the values of barrier height decrease with increasing light intensity, while the values of I_S and n increase. The production of other chargers by illumination increases the saturation reverse current [20]. With increasing illumination intensity, the increase in the values of

I_S and n indicate that the current passing through the junction does not obey to the thermionic emission theory, this process can be caused by an increase in conduction due to electrons freeing from surface states [21–26].

There is no evident that both shunt resistance (R_{sh}) and series resistance (R_S) are essential parameters that impact the performance and

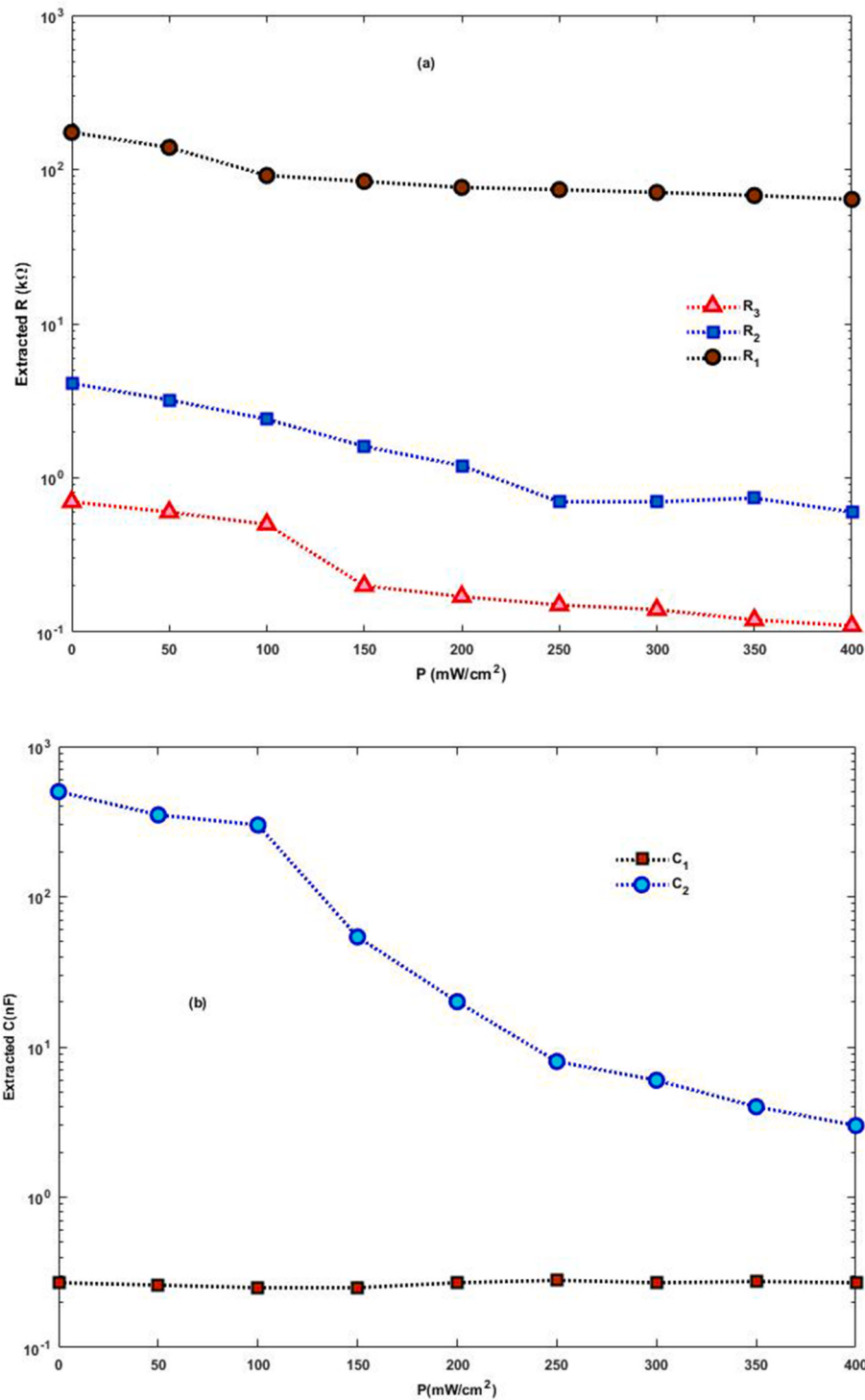


Fig. 7. Resistances (a) and capacitances (b) plots extracted from I_S best fit.

quality of the Schottky junction. R_S and R_{Sh} values are obtained from plots of the structural resistance (R_i) versus the applied voltage (V_i), using Ohm's law the structural resistance (R_i) can be computed by the following equation [27]:

$$R_i = dV_i/dI_i \quad (5)$$

Fig. 3 shows the voltage-dependent resistance profile of $Fe/n-Si_{0.35}Ge_{0.65}$ (MS) Schottky diode using Ohm's law (Eq. (5)). At sufficiently high forward bias ($V > 1.5V$), resistance corresponds to diode R_S value. On the other hand, at sufficiently high reverse bias ($V < -1.5V$),

resistance corresponds to diode shunt resistance (R_{Sh}) that is a measure of diode current leakage. As can be seen on Fig. 3, R_S is almost independent of light intensity while R_{Sh} is very dependent and it decrease with increasing illumination intensity. Estimated R_S value is about 69Ω while R_{Sh} values changed from $\sim 16 \times 10^5$ to $\sim 4 \times 10^5\Omega$ when we go from dark to $400mw/cm^2$ light intensity. This is associated to an increase in the density of free charge carriers resulting from rupture of bond or detrapping process [27,28].

It is also clear from Fig. 2 that the reverse current (I_R) exhibits an exponential dependence on applied reverse voltage (V_R), which suggests

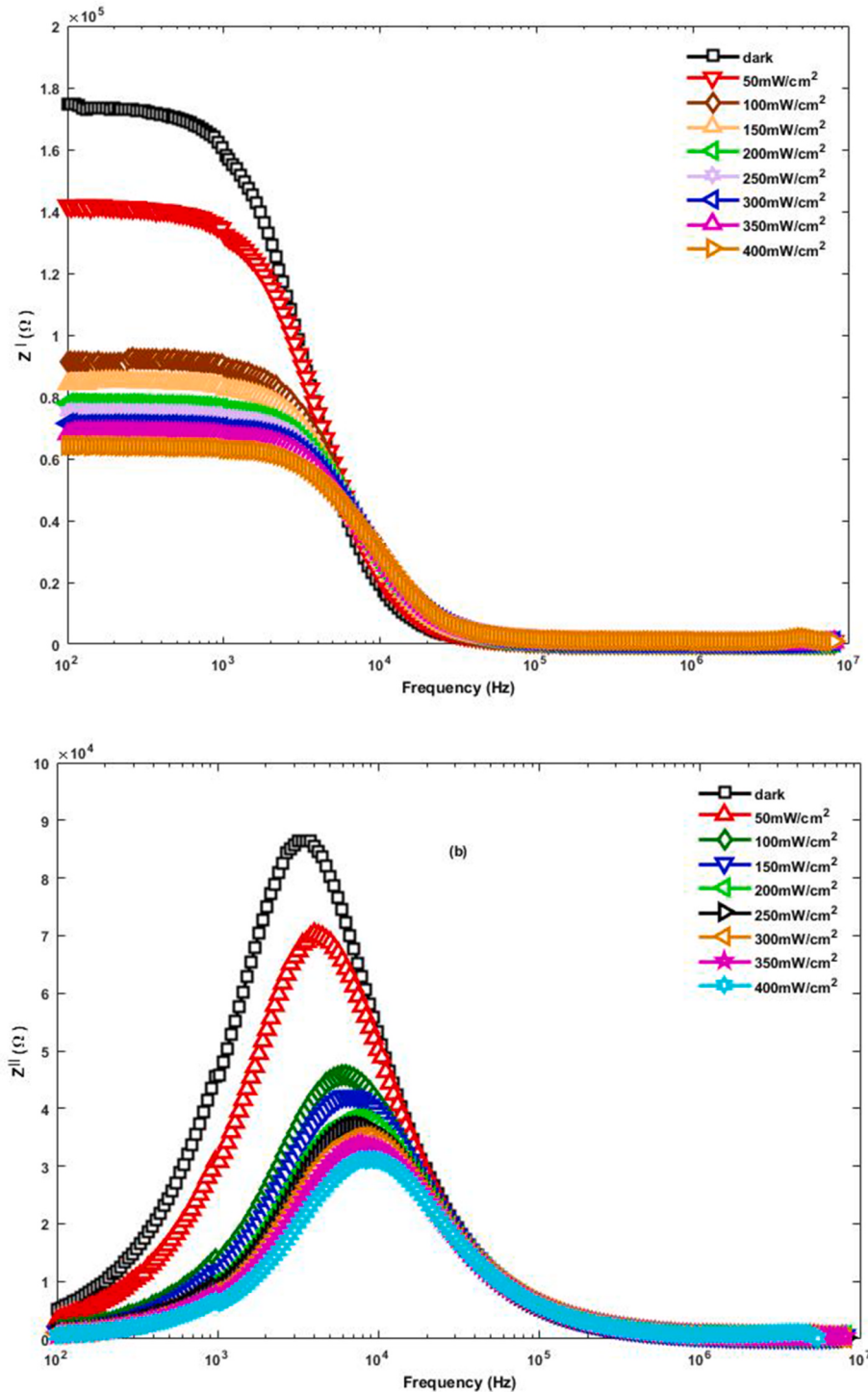


Fig. 8. Impedance behavior of Fe/n-Si_{0.65}Ge_{0.35} diode with light intensity: (a) real part Z' and (b) imaginary part Z'' .

that Fe/n-Si_{0.65}Ge_{0.35} Schottky contact is dominated by Poole-Frenkel or Schottky barrier lowering phenomena. The plots (I_R) Vs (V_R)^{1/2} have a linear variation, we believe that Schottky field-lowering at injecting electrode interface or Poole-Frenkel field-assisted thermal detrapping are responsible. The Poole-Frenkel emission current can be presented as [29–31]:

$$I_R = I_{PF} \exp \left[(\beta_{PF} / kT) \sqrt{(V_R/d)} \right] \quad (6)$$

When Schottky effect is dominated, it can be expressed as:

$$I_R = A * T^2 \exp \left(-\phi_S / kT \right) \exp \left[(\beta_{SC} / kT) \sqrt{(V_R/d)} \right] \quad (7)$$

Where $A *$ is Richardson constant, ϕ_S is metal semiconductor (MS) barrier height, k is Boltzmann constant, T is temperature, and V_R is reverse voltage. β_{PF} and β_{SC} are the Poole-Frenkel and MS field lowering coefficients, respectively. Theoretical values for β_{PF} and β_{SC} are given by:

$$\beta_{PF} = 2\beta_{SC} = (q^3 / (\pi\epsilon\epsilon_0))^{1/2} \quad (8)$$

Poole-Frankel coefficient can be obtained from the extracted values

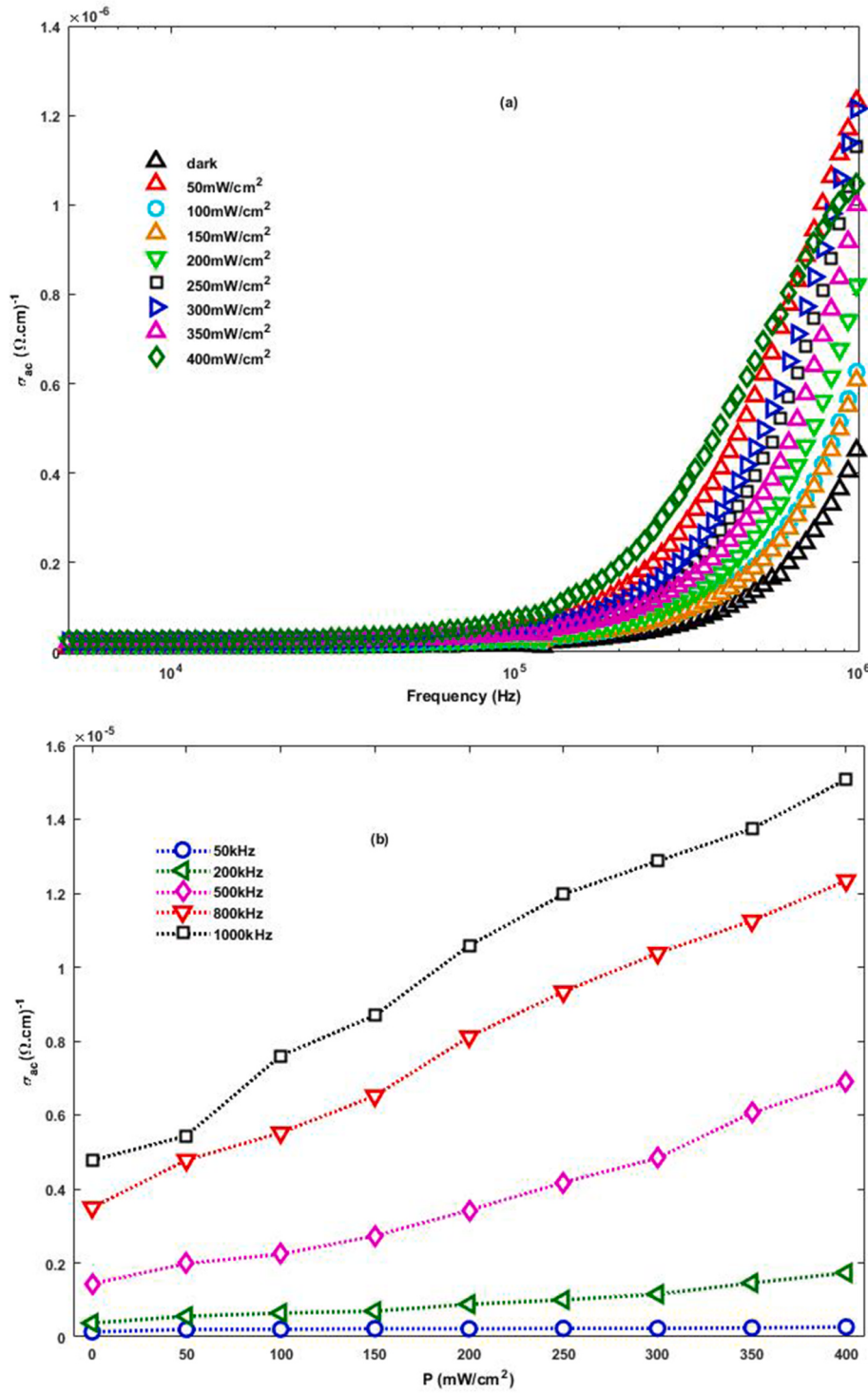


Fig. 9. Fe/n-Si_{0.65}Ge_{0.35} ac conductivity behaviour plotted (a) versus frequency (b) versus light intensity.

of field-lowering coefficients. β_{PF} is twice the value of β_{SC} . For *Fe/n-Si_{0.65}Ge_{0.35}* Schottky contacts, theoretical β_{PF} and β_{SC} calculated from Eq. (8) are 2.11×10^{-5} and $1.05 \times 10^{-5} \text{ eV m}^{1/2} V^{-1/2}$, respectively.

The parameters (β_{PF} or β_{SC}) were extracted from the slope of linear fit of $\ln(I_R)$ versus $V_R^{1/2}$ plots as shown on Fig. 4. The obtained values are $4.08 \times 10^{-5} \text{ eVm}^{1/2} V^{-1/2}$ in the dark and $1.2 \times 10^{-5}, 0.92 \times 10^{-5}, 0.71 \times 10^{-5}, 0.61 \times 10^{-5}$ for 100, 200, 300 and 400 mW/cm² respectively. Experimental results are compatible with theoretical value of β_{PF} in the dark and β_{SC} under light illumination. Therefore, Poole-Frenkel conduction mechanism is outstanding in dark and under low polarisation,

we believe that imperfection such as vacancies or dislocations are responsible for capture and release of charge carriers [32,33]. It is noted that under illumination and reverse bias, conduction mechanism of *Fe/n-Si_{0.65}Ge_{0.35}* Schottky diodes flow Schottky emission rather than Poole-Frenkel emission mechanism.

As can be seen from Fig. 2, At high forward bias voltages, current-voltage characteristics of MS diodes show a non-linearity indicating the presence of traps at semiconductor interface [34,35]. According to Refs. [36,37], ideality factor as a function of voltage can be written in the form:

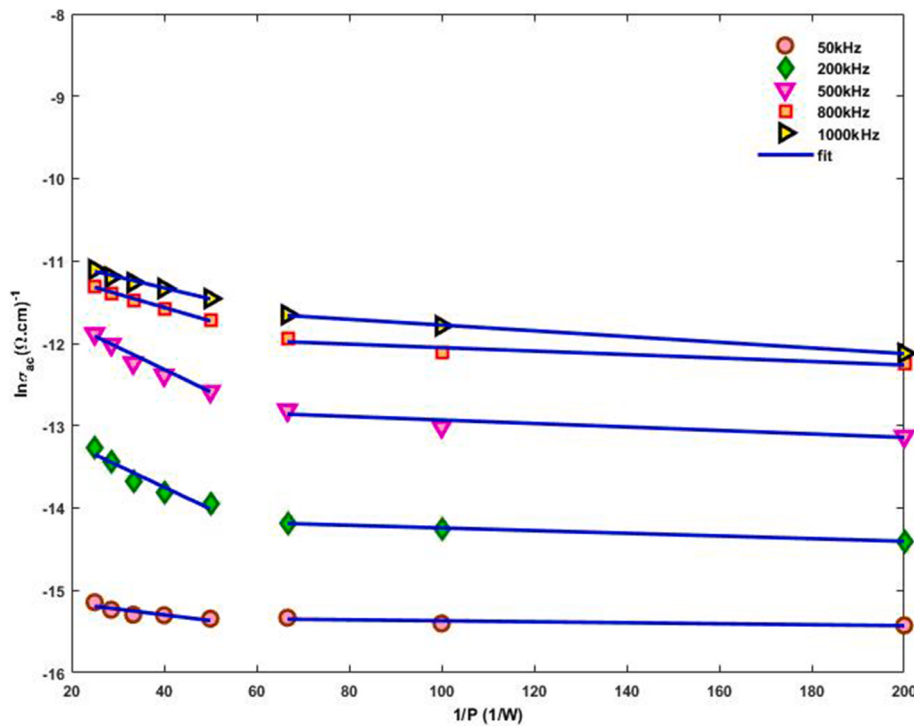
Fig. 10. $\ln \sigma_{ac}$ vs $1/P$ of Fe/n-Si_{0.65}Ge_{0.35} SBD.

Table 2
Activation energy and ac conductivity intercept extracted from $\sigma_{AC} - (1/E_u)$ plot.

Frequency	Region I		Region II	
	E_I (eV)	σ_I (Ωcm) ⁻¹	E_{II} (eV)	σ_{II} (Ωcm) ⁻¹
50 kHz	-0.45117	2.707×10^{-07}	-0.089	2.234×10^{-07}
200 kHz	-2.21308	2556×10^{-06}	-0.243	7.653×10^{-07}
500 kHz	-2.54198	1187×10^{-05}	-0.317	2.973×10^{-06}
800 kHz	-1.52062	1728×10^{-05}	-0.318	7210×10^{-06}
1000 kHz	-1.20409	1932×10^{-05}	-0.521	1087×10^{-05}

$$n(V) = 1 + (\delta / \epsilon_i) [\epsilon_s / W_D + qN_{SS}(V)] \quad (9)$$

Then interface states density (N_{SS}) can be determined from Eq. (9) as:

$$N_{SS}(V) = (1/q) [(\epsilon_i / \delta) (n(V) - 1) - \epsilon_s / W_D] \quad (10)$$

Where W_D is space charge width, ϵ_s ($= 12.93 \epsilon_0$) and ϵ_i ($= 3.8 \epsilon_0$) are relative permittivity of SiGe and interfacial layer, respectively, ϵ_0 is permittivity of free space and δ is the thickness of interfacial layer. W_D value for Fe/n-Si_{0.65}Ge_{0.35} diode was deduced from reverse bias Capacitance-Voltage measurement at 1 MHz frequency and was found to be 0.54 μm . The thicknesses of native insulator layers (SiO₂) at the interface “ δ ” for Fe/n-Si_{0.65}Ge_{0.3} was extracted from interfacial layer capacitance ($C_i = \epsilon_i \epsilon_0 A / \delta$) in strong accumulation region [14], δ are found to be 29.44 \AA .

The energy of surface states E_{SS} against the lowest of the conductance band (E_C) can be expressed by.:

$$E_C - E_{SS} = q(\Phi_e - V), \quad (11)$$

Where ϕ_e ($\Phi_e = \Phi_{B0} + (1 - 1/n(V))$) is the effective barrier height.

Fig. 5 shows interface state density distribution against the surface state energy for various light intensities. N_{SS} energy values of Fe/n-Si_{0.65}Ge_{0.35} SBD are in the range ($E_C - 0.40\text{eV}$) to ($E_C - 0.71\text{eV}$). N_{SS} present an exponential increase from mid-gap to lowest of conduction band. The surface density of N_{SS} at ($E_C - 0.40\text{eV}$) is $5.25 \times 10^{13} \text{ eV}^{-1}\text{cm}^{-2}$ in dark. It's clear that effective barrier height ϕ_e has increased. The finding has

many possible causes, namely an increase in quasi-Fermi energy level of semiconductor majority carriers. Thermionic emission current will be created by injecting electrons from semiconductor into metal, while a portion of electrons is captured by trap states. The recombination process minimise current diode and it increase effective barrier height diode [36,38]. As can be seeing, the values of N_{SS} increase with increasing illumination intensity between ($E_C - 0.43$) and ($E_C - 0.71$) eV.

3.2. Electrical impedance spectroscopy study

Impedance spectra of Fe/n-Si_{0.65}Ge_{0.35} Schottky contacts were extracted from 100 Hz to 1 MHz frequency range for light intensities from dark to 400 mW/cm² with a step of 50 mW/cm² at room temperature. Fig. 6 shows Cole-Cole impedance plots at 0.2V forward bias. The plots have a semicircle shape. The radius of the semicircle increases as illumination intensity decreases. It means that device impedance value is dependent on illumination intensity and it has a much larger value in the dark. The Schottky diode impedance has a semi-circular curve over the illumination intensity range, a parallel circuit of (R - C) can be used to model the diode [39,40]. Since Cole-Cole impedance plots of Fig. 6 are not perfect semi-circular shapes (in a low frequency region), we should present the junction structure by two RC circuits. Equivalent R-C circuit with series resistance that is shown in Fig. 6 has been used to model experimental results. In equivalent circuit model, inset of Fig. 6, capacitances C_1 and C_2 are related to space charge layer of Fe-Si_{1-x}Ge_x metal-semiconductor interfaces and bulk region, respectively, with corresponding shunt resistances R_1 and R_2 .

The total diode impedance is written as:

$$Z(\omega) = Z'(\omega) - jZ''(\omega), \quad (12)$$

The equivalent circuit for the diode in Fig. 6 leads to the Z' (ω) and Z'' (ω) to be written as [40,41]:

$$Z'(\omega) = R_1 / (1 + (\omega R_1 C_1)^2) + R_2 / (1 + (\omega R_2 C_2)^2) + R_3 \quad (13)$$

Extracted values of resistances and capacitances are plotted in Fig. 7a and Fig. 7b. R_3 decreases from 700 Ω in dark to 140 Ω at 400 mW/cm².

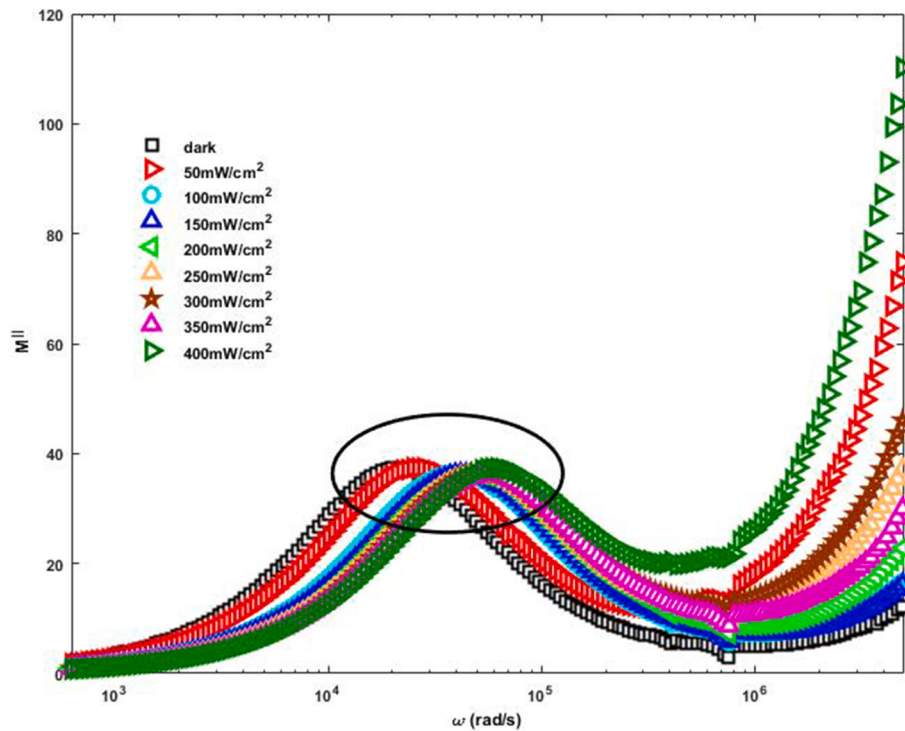


Fig. 11. Loss modulus (M'') vs angular frequency of Fe/n-Si_{0.65}Ge_{0.35} SBD.

R_2 shows a significant change with light intensity and decreased from $4\text{k}\Omega$ in dark to $0.6\text{k}\Omega$ at 400mW/cm^2 . Capacitance C_2 decreased from 500nF to 3nF when going from dark to 400mW/cm^2 . Resistance R_1 is less dependent on light intensity than R_2 with high values decreasing from $174\text{k}\Omega$ in dark to $64\text{k}\Omega$ at 400mW/cm^2 . Capacitance C_1 is almost constant and its average value is 0.3nF . The Fe/n-Si_{0.65}Ge_{0.35} interface was modeled by an R_1C_1 equivalent circuit. The equivalent circuit is due to surface imperfections such as defects at the interface. R_2C_2 component of proposed mode is related to the bulk region of Si_{0.65}Ge_{0.35} semiconductor.

Fig. 8a shows impedance real part Z' plotted against log of frequency at different light intensities. At lower frequency, the real part of Z' has a maximum value in dark and decrease with increasing intensity, at higher frequency Z' decreases gradually with increasing frequency, indicating a charges carriers release in space charge [42]. In low frequency region, Z' decrease with light intensity from $174\text{k}\Omega$ (in dark) to $68\text{k}\Omega$ (at 400mW/cm^2). Whereas, for frequencies above 1MHz , Z' spans a narrow range between 20\AA and 122\AA . In such region Z' seems to be independent of illumination intensities. At low frequencies, Z' follows space charge polarisation that changes with light intensities due to the increase in charge carriers mobility and/or decrease in trapped charges density. Fig. 8b shows impedance imaginary part Z'' plotted against log of frequency for different light intensities. The peak magnitude of Z'' decreases with increased light intensity. These peaks suggest the existence of relaxation processes in bulk and/or interface regions due to the interaction of mobile species with defects and vacancies for various illumination intensities [43,44]. With increased light intensity, Z'' peak magnitude decreased and all peaks are shifted towards higher frequency. Above 1MHz , all plots converge to the same value. At higher frequencies, the space charge effect fading, the only contribution is the bulk resistance effect [45].

3.3. Electrical conductivity of Fe/n-Si_{0.35}Ge_{0.65}

Electrical conductivity (σ_{ac}) variation at different frequencies for illuminations ranging from dark to 400mW/cm^2 at room temperature for

Fe/n-Si_{0.65}Ge_{0.35} SBDs is shown in Fig. 9a. The results show an increase in ac conductivity, especially for frequencies above 10^5Hz , in good agreement with reported Chenari results [46]. It is known that hopping of charge carriers can be enhanced by increasing frequency [47]. Such ac electrical conductivity can be evaluated from [49]:

$$\sigma_{ac}(\omega) = (\delta / A) (Z' / (Z'^2 + Z''^2)) \quad (15)$$

Where δ is the thickness and A is diode effective area. This ac conductivity depends greatly upon the impedance real part (Z') and consequently explains the observed ac conductivity increase. The variation of conductivity σ_{ac} as a function of frequency is widely discussed in the literature, this variation is due to the series resistance effect [43].

Fig. 9b shows σ_{ac} versus light intensity at five chosen frequency values. Photoconductivity is shown and it increases with increasing frequency [48–50]. Several factors can contribute to the increase in conductivity, we can cite the polarisation relaxation processes that can be enhanced by high frequency and the charge carriers hoping between traps at high ac frequency [51,52].

Fig. 10 shows another relation between light intensity and ac conductivity for Fe/n-Si_{0.35}Ge_{0.65}. Here, the ac conductivity shows a linear variation with a negative slope as a function of the inverse of the light intensity. We think that two kinds of charge transport mechanisms occur, one corresponding to the region (I) and another corresponding to the region (II). The total conductivity through Fe/n-Si_{0.35}Ge_{0.65} can be written as:

$$\sigma(1/E_u) = \sigma_I \exp(-E_I/E_u) + \sigma_{II} \exp(-E_{II}/E_u) \quad (16)$$

Where σ_I and σ_{II} are constants and E_I and E_{II} are activation energies for each electrical conductivity region. E_U is illumination energy ($E_U = P \times \Delta t$; where Δt is sample exposition time to illumination during measurement). Extracted parameters were listed in Table 2. Conductivity through Fe/n-Si_{0.35}Ge_{0.65} increases steadily up to a certain illumination intensity.

Conductivity Vs illumination intensity obeys Arrhenius relationship in both regions. A hopping phenomena in conduction was observed at 1/

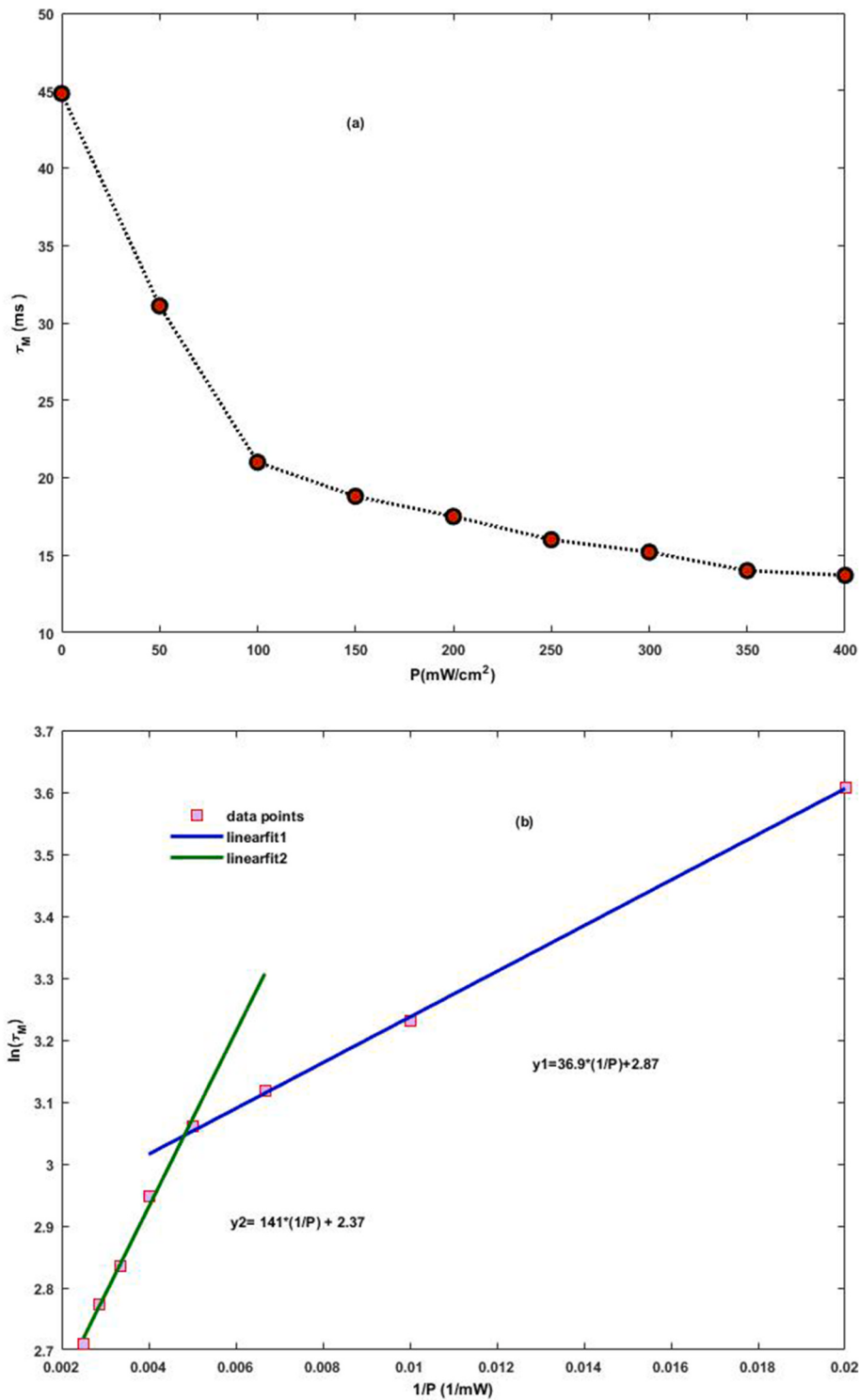


Fig. 12. (a) Relaxation time (τ_M) versus illumination intensities and (b) $\ln(\tau_M)$ vs $(1/P)$ of Fe/n-Si_{0.65}Ge_{0.35} SBD.

$p = 5W^{-1}$. The observed hopping in conductivity can related to phase transition caused by physical or structural changes [14]. In the regions I (200–400 mW/cm²), we believe that the excitation of charge carriers by light is the main factor that drives the conductivity to obey the Arrhenius formula. The activation energy in region II (50–150) mW/cm² is lower than in the region I (see table 0.2), it increases at a lower rate and the conductivity is due to the lower illumination excitation of charge carriers.

Electrical modulus is another important parameter as formulated by

Macedo et al. [53]. The complex formula of electric modulus can be expressed by:

$$M^*(\omega) = M' + iM'' \quad (17)$$

where $M' = \omega C_0 Z''$, and $M'' = \omega C_0 Z'$.

C_0 is geometrical capacitance. the imaginary (M'') part of the complex modulus versus ω curves (Fig. 11) shows a broad peak that shifts towards higher frequencies with increasing illumination intensity. These peaks are basically related to light-dependent relaxation processes [54].

The maximum angular frequency ω_{\max} ($= 2\pi f_{\max}$) corresponding to M''_{\max} (maximum value of M'') is the reciprocal of relaxation time, τ_M [55] as:

$$\omega_{\max} = 1/\tau_M \quad (18)$$

At different illumination intensities, this ω_{\max} is different and increases with increasing illumination intensity (Fig. 12a). Relaxation time has been analyzed using equation:

$$\tau_M = \tau_0 \exp(E_a / E_u) \quad (19)$$

Where τ_0 is pre-exponential factor, E_U is illumination energy, E_a is activation energy [56]. The variation of τ_M as a function of inverse of power illumination intensity ($1/P$) is shown in Fig. 12b. It appears to be linear and follows Arrhenius relation given in Eq (19). The activation energy is calculated from the slope of $\log(\tau_M)$ against $1/P$ curves ($Slope = E_a/\Delta t$). Average sample exposure time to illumination during measurement was 15s. The pre-exponential factor τ_0 extracted from y-intercept. Fig. 12b shows two distinct linear regions. Hence, activation energy and pre-exponent are 0.553 eV and 10.67 ms in the region I (50–200 mW) and 2.11eV and 17.63 ms in region II (250–400 mW), respectively.

4. Conclusion

Effects of illumination and frequency on the main electric properties of $Fe/n-Si_{0.65}Ge_{0.35}$ SBDs are discussed. Experimental results analysis shows that $I-V$ characteristics, real and imaginary part of the complex impedance (Z , Z''), electric modulus (M'') and ac electrical conductivity (σ_{ac}) are strongly dependent on both illumination intensity and frequency indicating light induced activity in depletion and interface regions. $I-V$ plots show a kind of photovoltaic effect due to electron-hole pairs' generation that are separated by the depletion local electric field. All electrical parameters such as ideality factor, barrier height, series and shunt resistance, and density of interface states extracted from $I-V$ measurement are strongly dependent on illumination intensity. Cole-Cole plots of (Z , Z'') led to propose an equivalent circuit model for the diode with circuit elements values extracted from experimental results. Decrease in Z' value, at low frequencies, with illumination intensity is due to the increase in mobility of charge carriers and/or the decrease in the density of trapped charges. The appearance of peaks in Z'' vs frequency in high illumination intensity region suggests the existence of relaxation process at the interface and probably in bulk. σ_{ac} increase with increasing frequency and illumination intensity is attributed to electric energy associated with high ac frequency that can effectively promote charge carriers jumping between traps. Calculated relaxation time obeys Arrhenius formula and is used to calculate activation energy of traps in the interface layer.

CRediT authorship contribution statement

Abdelkader Teffahi: Writing – review & editing, Writing – original draft, Validation, Project administration, Investigation, Formal analysis, Conceptualization. **Djillali Hamri:** Writing – review & editing, Writing – original draft, Methodology, Investigation, Funding acquisition, Formal analysis, Data curation. **Asma Djeghlouf:** Methodology, Formal analysis. **Abdelkader Mostefa:** Writing – review & editing, Conceptualization. **Mahmoud Arbid:** Writing – review & editing. **Souleyman Benkraouda:** Writing – review & editing. **Abdelmadjid Mesli:** Writing – review & editing.

Ethics statement

I, the Corresponding Author, declare that this manuscript is original, has not been published before and is not currently being considered for publication elsewhere.

I can confirm that the manuscript has been read and approved by all named authors and that there are no other persons who satisfied the criteria for authorship but are not listed. I further confirm that the order of authors listed in the manuscript has been approved by all of us.

I understand that the Corresponding Author is the sole contact for the Editorial process and is responsible for communicating with the other authors about progress, submissions of revisions and final approval of proofs.

Signed by the Corresponding Author on behalf of the all other authors"

Declaration of competing interest

The authors declare that they have no known competing financial interests or personal relationships that could have appeared to influence the work reported in this paper.

Data availability

Data will be made available on request.

References

- [1] G.L. Zhou, H. Morkoç, Si/SiGe heterostructures and devices, *Thin Solid Films* 231 (1993) 125–142, [https://doi.org/10.1016/0040-6090\(93\)90708-W](https://doi.org/10.1016/0040-6090(93)90708-W).
- [2] H.-U. Schreiber, B.G. Bosch, E. Kasper, H. Kibbel, Si/SiGe heterojunction bipolar transistor with base doping highly exceeding emitter doping concentration, *Electron. Lett.* 3 (1989) 185–186, <https://doi.org/10.1049/el:19890134>.
- [3] W. Lu, A. Kuliev, S.J. Koester, X.-W. Wang, J.O. Chu, T.-P. Ma, I. Adesida, High performance 0.1/spl mu/m gate-length p-type SiGe MODFET's and MOS-MODFET's, *IEEE Trans. Electron. Dev.* 47 (2000) 1645–1652, <https://doi.org/10.1109/16.853043>.
- [4] H. Daembkes, H.-J. Herzog, H. Jorke, H. Kibbel, E. Kasper, The n-channel SiGe/Si modulation-doped field-effect transistor, *IEEE Trans. Electron. Dev.* 33 (1986) 633–638, <https://doi.org/10.1109/T-ED.1986.22544>.
- [5] T.-L. Lin, A. Ksendzov, S.M. Dejewski, E.W. Jones, R.W. Fathaure, T.N. Krabach, J. Maserjian, SiGe/Si heterojunction internal photoemission long-wavelength infrared detectors fabricated by molecular beam epitaxy, *IEEE Trans. Electron. Dev.* 38 (1991) 1141–1144, <https://doi.org/10.1109/16.78391>.
- [6] F. Meyer, V. Aubry, P. Warren, D. Dutartre, W/Si1-xGex Schottky barrier: effect of stress and Composition, *MRS Online Proc. Libr.* 338 (1994) 167, <https://doi.org/10.1557/PROC-338-167>.
- [7] M. Mamor, F.D. Auret, S.A. Goodman, G. Myburg, Electrical characterization of defects introduced in p-Si1-xGex during electron-beam deposition of Sc Schottky barrier diodes, *Appl. Phys. Lett.* 72 (1998) 1069–1071, <https://doi.org/10.1063/1.120967>.
- [8] S.S. Iyer, G.L. Patton, J.M.C. Stork, B.S. Meyerson, D.L. Harame, Heterojunction bipolar transistors using Si-Ge alloys, *IEEE Trans. Electron. Dev.* 36 (1989) 2043–2064, <https://doi.org/10.1109/16.40887>.
- [9] C. Wang, M. Zhang, W. Xia, High-temperature dielectric relaxation in Pb(Mg1/3Nb2/3)O3-PbTiO3 single crystals, *J. Am. Ceram. Soc.* 96 (2013) 1521–1525, <https://doi.org/10.1111/jace.12210>.
- [10] C. Yim, N. McEvoy, G.S. Duesberg, Characterization of graphene-silicon Schottky barrier diodes using impedance spectroscopy, *Appl. Phys. Lett.* 103 (2013) 193106, <https://doi.org/10.1063/1.4829140>.
- [11] I. Dökme, Ş. Altindal, T. Tunç, İ. Uslu, Temperature dependent electrical and dielectric properties of Au/polyvinyl alcohol (Ni, Zn-doped)/n-Si Schottky diodes, *Microelectron. Reliab.* 50 (2010) 39–44, <https://doi.org/10.1016/j.microrel.2009.09.005>.
- [12] I.M. Hodge, M.D. Ingram, A.R. West, Impedance and modulus spectroscopy of polycrystalline solid electrolytes, *J. Electroanal. Chem. Interfacial Electrochem.* 74 (1976) 125–143, [https://doi.org/10.1016/S0022-0728\(76\)80229-X](https://doi.org/10.1016/S0022-0728(76)80229-X).
- [13] M. Willander, O. Nur, N. Bano, K. Sultana, Zinc oxide nanorod-based heterostructures on solid and soft substrates for white-light-emitting diode applications, *New J. Phys.* 11 (2009) 125020, <https://doi.org/10.1088/1367-2630/11/12/125020>.
- [14] G. Amin, S. Zaman, A. Zainelabdin, O. Nur, M. Willander, ZnO nanorods–polymer hybrid white light emitting diode grown on a disposable paper substrate, *Phys. Status Solidi Rapid Res. Lett.* 5 (2011) 71–73, <https://doi.org/10.1002/pssr.201004446>.
- [15] J.A. Anta, E. Guillén, R. Tena-Zaera, ZnO-based dye-sensitized solar cells, *J. Phys. Chem. C* 116 (2012) 11413–11425, <https://doi.org/10.1021/jp3010025>.
- [16] D. Hamri, A. Teffahi, A. Djeghlouf, A. Saidane, A. Mesli, Temperature dependent transport characterization of iron on n-type (111) $Si_{0.65}Ge_{0.35}$ Schottky diodes, *J. Alloys Compd.* 763 (2018) 173–179, <https://doi.org/10.1016/j.jallcom.2018.05.336>.
- [17] S.M. Sze, K.K. Ng, *Physics of Semiconductor Devices*, John Wiley & Sons, 2006.
- [18] E.H. Rhoderick, Metal-semiconductor contacts, *IEE Proceed. I Solid State Electron Dev.* 129 (1982) 1, <https://doi.org/10.1049/ip-i-1.1982.0001>.

- [19] M. Çavaş, F. Yakuphanoglu, Ş. Karataş, The electrical properties of photodiodes based on nanostructure gallium doped cadmium oxide/p-type silicon junctions, Indian J. Phys. 91 (2017) 413–420, <https://doi.org/10.1007/s12648-016-0952-4>.
- [20] Ş. Karataş, N. Berk, Performance of the illumination dependent electrical and photodiode characteristic of the Al/(GO:PTCDA)/p-Si structures, Opt. Mater. 126 (2022) 112231, <https://doi.org/10.1016/j.optmat.2022.112231>.
- [21] M. Gökçen, Ş. Altindal, M. Karaman, U. Aydemir, Forward and reverse bias current–voltage characteristics of Au/n-Si Schottky barrier diodes with and without SnO₂ insulator layer, Phys. B Condens. Matter 406 (2011) 4119–4123, <https://doi.org/10.1016/j.physb.2011.08.006>.
- [22] V. Rajagopal Reddy, A. Umapathi, L. Dasaradha Rao, Effect of annealing on the electronic parameters of Au/poly(ethylmethacrylate)/n-InP Schottky diode with organic interlayer, Curr. Appl. Phys. 13 (2013) 1604–1610, <https://doi.org/10.1016/j.cap.2013.06.001>.
- [23] S. Sönmezoglu, S. Şenkul, R. Taş, G. Çankaya, M. Can, Electrical and interface state density properties of polyaniline–poly-3-methyl thiophene blend/p-Si Schottky barrier diode, Solid State Sci. 12 (2010) 706–711, <https://doi.org/10.1016/j.solidstatesciences.2010.02.001>.
- [24] M. Gökçen, T. Tunç, Ş. Altindal, İ. Uslu, Electrical and photocurrent characteristics of Au/PVA (Co-doped)/n-Si photoconductive diodes, Mater. Sci. Eng., B 177 (2012) 416–420, <https://doi.org/10.1016/j.mseb.2012.01.004>.
- [25] İ. Dökme, T. Tunç, İ. Uslu, Ş. Altindal, The Au/polyvinyl alcohol (Co, Zn-doped)/n-type silicon Schottky barrier devices, Synth. Met. 161 (2011) 474–480, <https://doi.org/10.1016/j.synthmet.2011.01.002>.
- [26] V.R. Reddy, M.S.P. Reddy, A.A. Kumar, C.-J. Choi, Effect of annealing temperature on electrical properties of Au/polyvinyl alcohol/n-InP Schottky barrier structure, Thin Solid Films 520 (2012) 5715–5721, <https://doi.org/10.1016/j.tsf.2012.04.020>.
- [27] M. Yasan, M. Gökçen, A. Allı, S. Allı, Electrical characterization of Au/poly (linoleic acid)-g-poly(methyl methacrylate) (PLiMMA)/n-Si diode in dark and under illumination, Curr. Appl. Phys. 15 (2015) 14–17, <https://doi.org/10.1016/j.cap.2014.10.017>.
- [28] Ş. Karataş, M.G. Aydin, H. Özerli, Illumination impact on electrical properties of Ag/0.6 wt% nanographene oxide doped poly(vinyl alcohol) nanocomposite/p-Si heterojunction, J. Alloys Compd. 689 (2016) 1068–1075, <https://doi.org/10.1016/j.jallcom.2016.08.083>.
- [29] A.A. Kumar, V.R. Reddy, V. Janardhanam, M.-W. Seo, H. Hong, K.-S. Shin, C.-J. Choi, Electrical properties of Pt/n-Ge Schottky contact modified using copper phthalocyanine (CuPc) interlayer, J. Electrochem. Soc. 159 (2011) H33, <https://doi.org/10.1149/2.041201jes>.
- [30] A.S. Riad, Influence of dioxygen and annealing process on the transport properties of nickel phthalocyanine Schottky-barrier devices, Phys. B Condens. Matter 270 (1999) 148–156, [https://doi.org/10.1016/S0921-4526\(99\)00128-3](https://doi.org/10.1016/S0921-4526(99)00128-3).
- [31] V. Janardhanam, Y.-K. Park, K.-S. Ahn, C.-J. Choi, Carrier transport mechanism of Se/n-type Si Schottky diodes, J. Alloys Compd. 534 (2012) 37–41, <https://doi.org/10.1016/j.jallcom.2012.04.031>.
- [32] Z. Khurelbaatar, Y.-H. Kil, H.-J. Yun, K.-H. Shim, J.T. Nam, K.-S. Kim, S.-K. Lee, C.-J. Choi, Modification of Schottky barrier properties of Au/n-type Ge Schottky barrier diode using monolayer graphene interlayer, J. Alloys Compd. 614 (2014) 323–329, <https://doi.org/10.1016/j.jallcom.2014.06.132>.
- [33] A.C. Varghese, C.S. Menon, Electrical properties of hybrid phthalocyanines thin films using gold and lead electrodes, Eur. Phys. J. B 47 (2005) 485–489, <https://doi.org/10.1140/epjb/e2005-00352-7>.
- [34] A. Singh, K.C. Reinhardt, W.A. Anderson, Temperature dependence of the electrical characteristics of Yb/p-InP tunnel metal-insulator-semiconductor junctions, J. Appl. Phys. 68 (1990) 3475–3483, <https://doi.org/10.1063/1.346358>.
- [35] Ş. Karataş, F. Yakuphanoglu, Analysis of electronic parameters of nanostructure copper doped cadmium oxide/p-silicon heterojunction, J. Alloys Compd. 537 (2012) 6–11, <https://doi.org/10.1016/j.jallcom.2012.05.025>.
- [36] E.H. Rhoderick, Metal–Semiconductor Contacts, Oxford University Press, UK, 1978.
- [37] H. Özerli, A. Bekereci, A. Türüt, Ş. Karataş, Electrical and photovoltaic properties of Ag/p-Si structure with GO doped NiO interlayer in dark and under light illumination, J. Alloys Compd. 718 (2017) 75–84, <https://doi.org/10.1016/j.jallcom.2017.05.121>.
- [38] A. Turut, M. Saglam, H. Efeoglu, N. Yalcin, M. Yildirim, B. Abay, Interpreting the nonideal reverse bias C–V characteristics and importance of the dependence of Schottky barrier height on applied voltage, Phys. B Condens. Matter 205 (1995) 41–50, [https://doi.org/10.1016/0921-4526\(94\)00229-O](https://doi.org/10.1016/0921-4526(94)00229-O).
- [39] J.R. Macdonald, W.B. Johnson, Fundamentals of impedance spectroscopy, in: Impedance Spectroscopy, John Wiley & Sons, Ltd, 2005, pp. 1–26, <https://doi.org/10.1002/0471716243.ch1>.
- [40] J.T.S. Irvine, D.C. Sinclair, A.R. West, Electroceramics: characterization by impedance spectroscopy, Adv. Mater. 2 (3) (1990) 132–138, <https://doi.org/10.1002/adma.19900020304>.
- [41] C. August, Studies in Physical and Theoretical Chemistry Dielectric Physics—Elsevier Science Ltd, Elsevier Scientific Publishing Company, Amsterdam, 1980, 1980 110–129.
- [42] J. Suchanicz, The low-frequency dielectric relaxation Na0.5Bi0.5TiO3 ceramics, Mater. Sci. Eng., B 55 (1998) 114–118, [https://doi.org/10.1016/S0921-5107\(98\)00188-3](https://doi.org/10.1016/S0921-5107(98)00188-3).
- [43] H. Singh, A. Kumar, K.L. Yadav, Structural, dielectric, magnetic, magnetodielectric and impedance spectroscopic studies of multiferroic BiFeO3–BaTiO3 ceramics, Mater. Sci. Eng., B 176 (2011) 540–547, <https://doi.org/10.1016/j.mseb.2011.01.010>.
- [44] B. Behera, P. Nayak, R.N.P. Choudhary, Structural and impedance properties of KBa2V5O15 ceramics, Mater. Res. Bull. 43 (2008) 401–410, <https://doi.org/10.1016/j.materresbull.2007.02.042>.
- [45] B. Behera, P. Nayak, R.N.P. Choudhary, Study of complex impedance spectroscopic properties of LiBa2Nb5O15 ceramics, Mater. Chem. Phys. 106 (2007) 193–197, <https://doi.org/10.1016/j.matchemphys.2007.05.036>.
- [46] H. Mahmoudi Chenari, A. Hassanzadeh, M.M. Golzan, H. Sedghi, M. Talebian, Frequency dependence of ultrahigh dielectric constant of novel synthesized SnO₂ nanoparticles thick films, Curr. Appl. Phys. 11 (2011) 409–413, <https://doi.org/10.1016/j.cap.2010.08.011>.
- [47] S. Dussan, A. Kumar, J.F. Scott, R.S. Katiyar, Effect of electrode resistance on dielectric and transport properties of multiferroic superlattice: a impedance spectroscopy study, AIP Adv. 2 (2012) 032136, <https://doi.org/10.1063/1.4746026>.
- [48] A. Shehab, R.A.A. Allah, A.F. Basha, F.H.A. El-Kader, Electrical properties of gamma-irradiated, pure, and nickel chloride-doped polyvinyl alcohol films, J. Appl. Polym. Sci. 68 (1998) 687–698, [https://doi.org/10.1002/\(SICI\)1097-4628\(19980502\)68:5<687::AID-APP1>3.0.CO;2-K](https://doi.org/10.1002/(SICI)1097-4628(19980502)68:5<687::AID-APP1>3.0.CO;2-K).
- [49] C.A. Hogarth, M.J. Basha, Electrical conduction in cobalt-phosphate glasses, J. Phys. D Appl. Phys. 16 (1983) 869, <https://doi.org/10.1088/0022-3727/16/5/018>.
- [50] C. Muralidhar, P.K.C. Pillai, Resistivity behaviour of barium titanate (BaTiO₃)/polyvinylidene fluoride (PVDF) composite, J. Mater. Sci. Lett. 6 (1987) 439–440, <https://doi.org/10.1007/BF01756790>.
- [51] H. Zhang, D. Wang, C. Hu, X. Kang, H. Liu, Synthesis and magnetic properties of Sn1–xCo_xO₂ nanostructures and their application in gas sensing, Sensor. Actuator. B Chem. 184 (2013) 288–294, <https://doi.org/10.1016/j.snb.2013.04.085>.
- [52] J. Hays, A. Punnoose, R. Baldner, M.H. Engelhard, J. Peloquin, K.M. Reddy, Relationship between the structural and magnetic properties of Co-doped \$mathrm{Sn}\{mathrm{O}\}_{2}nanoparticles, Phys. Rev. B 72 (2005) 075203, <https://doi.org/10.1103/PhysRevB.72.075203>.
- [53] P.B. Macedo, C.T. Moynihan, R. Bose, Phys. Chem. Glasses 13 (1972) 171–179.
- [54] A.K. Jonscher, Dielectric relaxation in solids, J. Phys. D Appl. Phys. 32 (1999) R57, <https://doi.org/10.1088/0022-3727/32/14/201>.
- [55] C.T. Moynihan, L.B. Boesch, N.L. Laberge, Phys. Chem. Glasses 14 (1973) 122.
- [56] A. Karmakar, S. Majumdar, S. Giri, Polaron relaxation and hopping conductivity in LaMn_{1-x}Fe_xO₃, Phys. Rev. B 79 (2009) 094406, <https://doi.org/10.1103/PhysRevB.79.094406>.